



Ablation of PGC-1 β Results in Defective Mitochondrial Activity, Thermogenesis, Hepatic Function, and Cardiac Performance

Christopher J. Lelliott^{1,2}, Gema Medina-Gomez¹, Natasa Petrovic³, Adrienn Kis¹, Helena M. Feldmann³, Mikael Bjursell², Nadeene Parker¹, Keira Curtis¹, Mark Campbell¹, Ping Hu⁴, Dongfang Zhang⁴, Sheldon E. Litwin⁴, Vlad G. Zaha⁵, Kimberly T. Fountain⁵, Sihem Boudina⁵, Mercedes Jimenez-Linan¹, Margaret Blount¹, Miguel Lopez¹, Aline Meirhaeghe⁶, Mohammad Bohlooly-Y², Leonard Storlien², Maria Strömstedt², Michael Snaith², Matej Orešič⁷, E. Dale Abel⁵, Barbara Cannon³, Antonio Vidal-Puig^{1*}

1 Department of Clinical Biochemistry, University of Cambridge, Cambridge, United Kingdom, **2** AstraZeneca R&D, Mölndal, Sweden, **3** The Wenner-Gren Institute, Stockholm University, Stockholm, Sweden, **4** Division of Cardiology, University of Utah, Salt Lake City, Utah, United States of America, **5** Division of Endocrinology, Metabolism, and Diabetes and Program in Human Molecular Biology and Genetics, University of Utah, Salt Lake City, Utah, United States of America, **6** INSERM, Institut Pasteur de Lille, Lille Cedex, France, **7** VTT Technical Research Centre of Finland, Espoo, Finland

The transcriptional coactivator peroxisome proliferator-activated receptor-gamma coactivator-1 β (PGC-1 β) has been implicated in important metabolic processes. A mouse lacking PGC-1 β (PGC1 β KO) was generated and phenotyped using physiological, molecular, and bioinformatic approaches. PGC1 β KO mice are generally viable and metabolically healthy. Using systems biology, we identified a general defect in the expression of genes involved in mitochondrial function and, specifically, the electron transport chain. This defect correlated with reduced mitochondrial volume fraction in soleus muscle and heart, but not brown adipose tissue (BAT). Under ambient temperature conditions, PGC-1 β ablation was partially compensated by up-regulation of PGC-1 α in BAT and white adipose tissue (WAT) that lead to increased thermogenesis, reduced body weight, and reduced fat mass. Despite their decreased fat mass, PGC1 β KO mice had hypertrophic adipocytes in WAT. The thermogenic role of PGC-1 β was identified in thermoneutral and cold-adapted conditions by inadequate responses to norepinephrine injection. Furthermore, PGC1 β KO hearts showed a blunted chronotropic response to dobutamine stimulation, and isolated soleus muscle fibres from PGC1 β KO mice have impaired mitochondrial function. Lack of PGC-1 β also impaired hepatic lipid metabolism in response to acute high fat dietary loads, resulting in hepatic steatosis and reduced lipoprotein-associated triglyceride and cholesterol content. Altogether, our data suggest that PGC-1 β plays a general role in controlling basal mitochondrial function and also participates in tissue-specific adaptive responses during metabolic stress.

Citation: Lelliott C, Medina-Gomez G, Petrovic N, Kis A, Feldmann HM, et al. (2006) Ablation of PGC-1 β results in defective mitochondrial activity, thermogenesis, hepatic function, and cardiac performance. *PLoS Biol* 4(11): e369. DOI: 10.1371/journal.pbio.0040369

Introduction

Transcriptional coactivators (TCs) have emerged as key proteins that are capable of regulating entire metabolic networks [1]. TCs are often selective with respect to the repertoire of transcription factor partners. The mechanisms used to modulate transcription may vary according to the specific TC, their transcription factor partners, and the nucleic acid environment in which they operate. TCs provide an additional layer of control by facilitating temporal and tissue-specific regulation of metabolic pathways [1].

Peroxisome proliferator-activated receptor-gamma coactivator-1 α (PGC-1 α , previously known as PGC-1) [2] is involved in coordinating diverse organ-specific transcription programs. For example, PGC-1 α not only activates the thermogenic program in brown adipose tissue (BAT) in response to environmental cold exposure but also modulates the metabolic transition from the fed to the fasted state in the liver [2–4]. Two other PGC-1 α -related genes have subsequently been found, PGC-1-related coactivator (PRC) [5] and PGC-1 β (PERC/ERRL-1) [6–8]. All three family members share a similar basic structure; an N-terminal domain containing nuclear hormone receptor-interacting motifs (the LXXLL

motifs) and a C-terminal region containing RNA-binding motifs (RMM) and serine-arginine rich (RS) domains. Whereas PRC is primarily an activator of nuclear respiratory factor-

Academic Editor: Gregory S. Barsh, Stanford University School of Medicine, United States of America

Received: June 2, 2006; **Accepted:** September 5, 2006; **Published:** November 7, 2006

DOI: 10.1371/journal.pbio.0040369

Copyright: © 2006 Lelliott et al. This is an open-access article distributed under the terms of the Creative Commons Attribution License, which permits unrestricted use, distribution, and reproduction in any medium, provided the original author and source are credited.

Abbreviations: BAT, brown adipose tissue; Cox, cytochrome oxidase subunit; ES cell, embryonic stem cell; ETC, electron transport chain; HDL, high-density lipoprotein; HFD, high-fat diet; KEGG, kyoto encyclopedia genes and genomes; LDL, low-density lipoprotein; NE, norepinephrine; NS, not significant; OxPhos, oxidative phosphorylation; PGC, peroxisome proliferator-activated receptor-gamma coactivator; RER, respiratory exchange ratio; VLDL, very low-density lipoprotein; WAT, white adipose tissue; WT, wild-type

* To whom correspondence should be addressed. E-mail: ajv22@cam.ac.uk

 These authors contributed equally to this work.

1 [5], PGC-1 α and PGC-1 β have a broader repertoire of partners [7,9–12].

The gene expression level of PRC is conserved between tissues [5], but the highest expression of PGC-1 α and PGC-1 β is found in oxidative tissues, including BAT, heart, and skeletal muscle [2,6,7]. However, despite this overlap of expression pattern, PGC-1 α and -1 β display different responses to physiological stimuli. Whereas PGC-1 α is transcriptionally up-regulated in BAT and skeletal muscle during cold exposure, PGC-1 β expression remains stable under these conditions [2,6,7]. Furthermore, up-regulation of PGC-1 α is essential for a normal response to acute cold exposure, indicating that PGC-1 β is not able to compensate for all aspects of a lack of PGC-1 α [13,14]. Similarly PGC-1 α is up-regulated in liver in response to fasting, whereas PGC-1 β expression remained stable [6,7,9], further suggesting that PGC-1 α is more often regulated transcriptionally than PGC-1 β .

Overexpression studies both in vivo and in vitro have revealed that both PGC-1 α and -1 β are capable of stimulating mitochondrial biogenesis, increasing mitochondrial oxygen consumption, and elevating gene expression of fatty acid oxidation and mitochondrial electron transport chain (ETC) components [7,9,15]. In addition, bioenergetic studies of C2C12 myotubes demonstrated that overexpression of PGC-1 α or -1 β enhances mitochondrial proton leak [15]. Thus PGC-1 β increases mitochondrial energy production through a combination of activated fatty acid oxidation gene expression with increased mitochondrial activity. A role for PGC-1 β enhancing mitochondrial activity is further supported by the fact that transgenic overexpression of PGC-1 β in mice results in elevated energy expenditure, resistance to high-fat diet (HFD), and genetically induced obesity [10].

Despite their functional similarities, it has recently been suggested that PGC-1 α and -1 β may have differing metabolic roles in liver. PGC-1 α stimulates expression of gluconeogenic genes both in vivo and in vitro [3,9,13,16], and based on data from mice exposed to a diet enriched in saturated fat for a short period of time, it appears that PGC-1 β but not PGC-1 α interacts with SREBP and LXR α to enhance hepatic lipogenesis and lipoprotein secretion [11]. In addition, PGC-1 β interacts with Foxa2 to facilitate hepatic secretion of very low density lipoprotein (VLDL) [17], suggesting a central role for PGC-1 β in hepatic lipid metabolism. The second organ where PGC-1 α and -1 β are also highly expressed is the heart [2,6], but only the role of PGC-1 α in cardiac energy metabolism has been studied in detail. Overexpression of PGC-1 α in cardiac muscle in vivo leads to uncontrolled mitochondrial proliferation, leading to cardiomyopathy and congestive heart failure due to contractile dysfunction [18,19]. Similarly, PGC-1 α knockout mice also develop heart failure with abnormal heart rate and impaired ventricular function [14,20], again suggesting that despite their similar mode of action, PGC-1 β is unable to compensate fully for a lack of PGC-1 α .

To investigate the function of PGC-1 β , we have generated and phenotyped a mouse model lacking PGC-1 β (the PGC1 β KO mouse). Using a combination of physiological experiments guided by a systems biology approach, we showed that PGC-1 β plays a general role in regulating the mitochondrial activity in tissues with active oxidative metabolism. In all tissues studied, lack of PGC-1 β was associated with a reduction in the expression of mitochon-

drial genes, including intermediary subunits and enzymes connected to ETC and oxidative phosphorylation (OxPhos). Despite these mitochondrial defects, the PGC1 β KO mouse was able to cope when challenged with a range of physiological stressors including cold acclimatisation and adrenergically-mediated BAT and cardiac stimulation but with abnormal compensatory responses. Altogether, these data suggest that PGC-1 β is an important regulator of basal energy homeostasis and essential for the proper metabolic tuning in acute stress situations in multiple organs.

Results

Generation of a PGC1 β KO Mouse

A conditional PGC1 β KO was generated using a triple LoxP targeting vector (Figure 1A) as detailed in the Material and Methods. Murine PGC-1 β is alternatively spliced at the 5' end [7] and at exon 4 [8,10]. Exons 4 and 5, which encode two of the nuclear hormone receptor interacting motifs (LXXLL), were deleted. Ablation of these exons also introduced a premature stop codon. PCR and Southern analyses of the selected clone confirmed the presence of the single LoxP in intron 5 and that the embryonic stem (ES) cell clone contained all three LoxP sites as designed (Figure 1B and 1C). Germ line transmission of the modified *PGC-1 β* allele was confirmed by PCR analysis of the *agouti* pups obtained from chimeras bred to C57BL/6 wild-type (WT) mice. Heterozygous triple-LoxP-containing mice were then bred with ROSA26-Cre mice to generate mice heterozygous for the PGC-1 β deletion. Total LoxP site recombination was detected using PCR from genomic DNA (Figure 1D) and RT-PCR from isolated RNA. Intercross breeding of heterozygous germ-line knockout animals produced litters that did not deviate significantly from the expected Mendelian ratio of genotypes, and the size of litters from PGC1 β KO heterozygous crosses was normal (averaging seven to eight pups per breeding event per female).

Effect of PGC-1 β Ablation on Energy Balance: Reduced Body Weight and WAT Content Consistent with Increased Energy Expenditure

No differences in food intake, total energy intake, total energy output as faeces, and no change in the ratio of energy in (as food) to energy out (as faeces) (Table S1) were detected in 12-wk-old male mice selected for equal body weight. Oxymax analysis revealed increased minimum metabolic rate at 22 °C in 9-wk-old male PGC1 β KO mice (Table 1). No differences in spontaneous activity (unpublished data) or in respiratory exchange ratio (RER) were detected, suggesting that there was no difference in whole-body substrate-type utilization. Consistent with an elevated minimum metabolic rate at ambient temperature, PGC1 β KO mice weighed less than their WT littermates (Figure 2A). A similar pattern was also observed in female PGC1 β KO mice.

Body composition analysis using dual energy x-ray absorptiometry (DEXA) confirmed decreased body weight at the expense of fat mass rather than lean mass in both young (8-wk) and older (27-wk) male PGC1 β KO mice compared to WT littermates (Figure 2B). This was confirmed in an independent group of weight-matched 14-wk-old male PGC1 β KO mice that had smaller gonadal adipose tissue depots than WT littermates. Other organs examined did not show differences

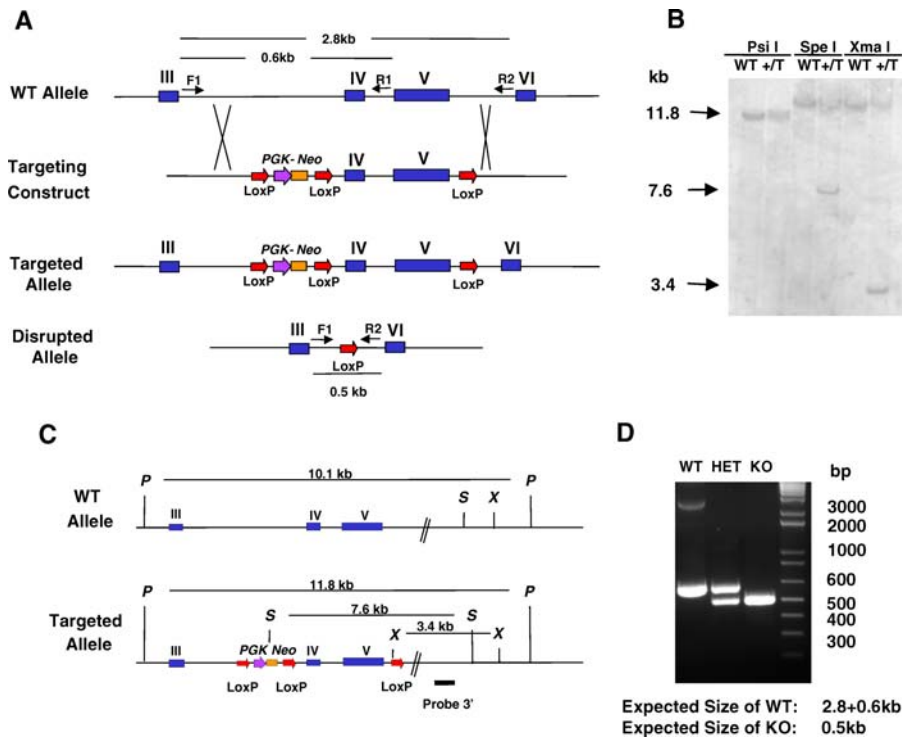


Figure 1. Generation of the PGC1 β KO Mouse

(A) Design of the targeting construct for the generation of the PGC1 β KO mouse using a phosphoglycerate kinase-neomycin phosphotransferase (PGK-Neo)-based LoxP cassette inserted between exons III and IV and a third LoxP site between exons V and VI. Total collapse of the LoxP sites deletes exons 4 and 5 of the *PGC-1 β* gene.

(B) A Southern blot confirming the generation of the targeted allele in ES cells. WT, wild type ES cells; +/T, ES cells heterozygous for the targeted allele, T.

(C) Schematic showing the restriction digest strategy for the southern blot confirming the generation of the targeted allele in ES cells. P, PstI; X, XmaI; S, SpeI.

(D) Confirmation of the total LoxP collapse and generation of KO mice by PCR from genomic DNA using primers F1, R1, and R2 shown in (A).

DOI: 10.1371/journal.pbio.0040369.g001

in their weights relative to body weight (Table S2). Histological analysis of male gonadal WAT from PGC1 β KO mice showed a reduced fraction of small adipocytes (up to an area of 2,000 μm^2) and an elevated fraction of larger adipocytes in the PGC1 β KO WAT (Figure 2C and 2D). This pattern for larger white adipocytes was also seen in male subcutaneous and omental WAT and in female gonadal WAT (Figure S1).

Therefore, when on a chow diet, the PGC1 β KO mice had less total WAT content than WT did, but it was composed of larger adipocytes. Histological analysis of other metabolically relevant tissues—including BAT, liver, skeletal muscle, and pancreas—did not reveal morphological alterations in PGC1 β KO mice under basal conditions (Figure S2).

Gene expression analysis of gonadal WAT from male

Table 1. Assessment of Energy Expenditure on 9-wk-Old Male Chow-Fed PGC1 β KO and WT Mice

Measurement	9-wk-old WT	9-wk-old PGC1 β KO	<i>p</i> Value
Minimum VO_2 (ml/min)	0.39 \pm 0.05	0.52 \pm 0.03	<i>p</i> = 0.07
Maximum VO_2 (ml/min)	1.47 \pm 0.06	1.40 \pm 0.05	NS
Minimum VO_2 (ml/kg/min)	16.1 \pm 2.3	22.6 \pm 1.8	<i>p</i> = 0.05
Maximum VO_2 (ml/kg/min)	59.9 \pm 1.7	60.8 \pm 3.0	NS
Minimum VO_2 (ml/kg[lean]/min)	20.0 \pm 2.7	27.3 \pm 2.0	<i>p</i> = 0.05
Maximum VO_2 (ml/kg[lean]/min)	74.5 \pm 2.0	73.5 \pm 3.2	NS
Minimum VO_2 (ml/kg ^{0.75} /min)	6.4 \pm 0.9	8.8 \pm 0.6	<i>p</i> = 0.05
Maximum VO_2 (ml/kg ^{0.75} /min)	23.7 \pm 0.7	23.7 \pm 1.0	NS
RER	0.88 \pm 0.01	0.90 \pm 0.01	NS

Oxygen consumption and the respiratory exchange ratio of male WT and PGC1 β KO mice was measured at 9 wk old, in mice housed and measured at 22 °C. Minimum values refer to the average of the three lowest VO_2 value recorded during the final 24 h of the experimental procedure, with maximum values referring to those corresponding to the highest three values of VO_2 during this period. VO_2 measurements are given related per mouse (ml/min) to total body weight (ml/kg/min), lean body weight (ml/kg [lean]/min), and using the scaling factor of 0.75 (ml/kg^{0.75}/min). The RER was calculated as the average RER measurement during the final 24 h of the procedure. *n* = 5–7 mice per group.

NS, not significant.

DOI: 10.1371/journal.pbio.0040369.t001

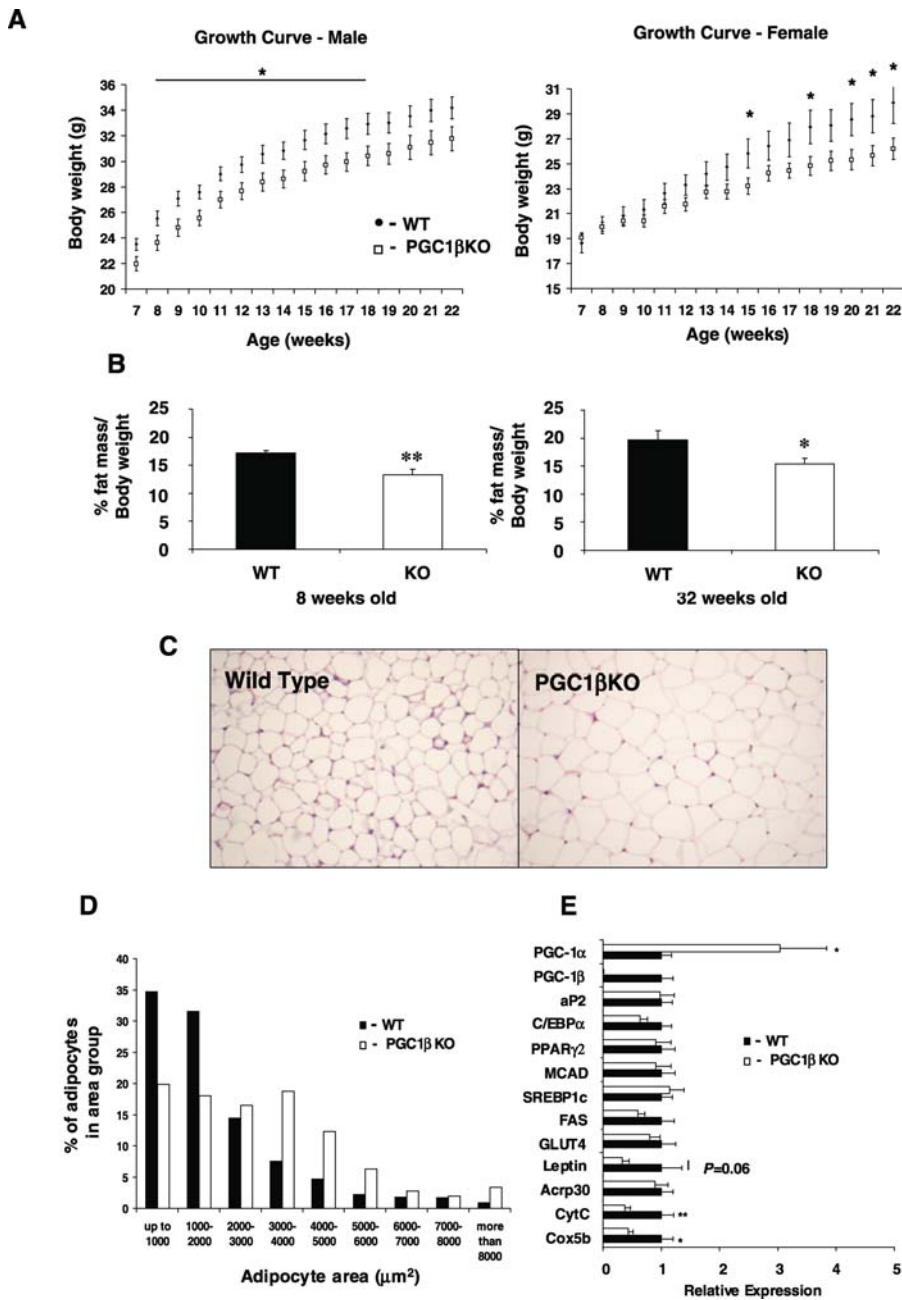


Figure 2. The PGC1 β KO Mouse Has Altered Metabolism under Standard Environmental Conditions

(A) Growth curves of male (left panel) and female (right panel) mice on normal diet. WT (solid circles) and PGC1 β KO (open circles) mice, $n = 18-21$ mice per group.

(B) Assessment of fat content by DEXA in 8- and 32-wk-old male WT (solid bars) and PGC1 β KO mice (open bars), $n = 8-12$ mice per group.

(C) Representative histological sections of tissues from WAT ($n = 6$).

(D) Size distribution of adipocytes from WT and PGC1 β KO mice. Two fields from each section from epididymal adipose tissue depot ($n = 4$ mice per genotype) were analysed to obtain the mean cell area per animal.

(E) Epididymal WAT gene expression from 12-wk-old PGC1 β KO (white bars) and WT littermates (black bars). Individual measurements are standardized using 18S, and then the average of the WT group was set to 1. $n = 5-8$ mice per group.

DOI: 10.1371/journal.pbio.0040369.g002

PGC1 β KO mice and WT littermates showed no significant change in markers of adipogenesis including C/EBP α , PPAR γ 2, aP2, and GLUT4 (Figure 2E). There was a significant up-regulation of PGC-1 α expression in WAT in the absence of PGC-1 β (Figure 2E). Previously, increased PGC-1 α expression in WAT has been associated with the development of a BAT-like phenotype [21]. However, increased expression of

PGC-1 α was not sufficient to increase *UCPI* and *D2-deiodinase* expression in PGC1 β KO WAT (unpublished data). Combined with the WAT morphology data, elevation of PGC-1 α in the PGC1 β KO WAT is not enough to result in clear BAT-like adipose tissue. However, ablation of PGC-1 β resulted in reduced expression in the ETC genes *CytC* and *Cytochrome Oxidase* subunit (*Cox*) *5b* and also in *leptin* ($p = 0.06$).

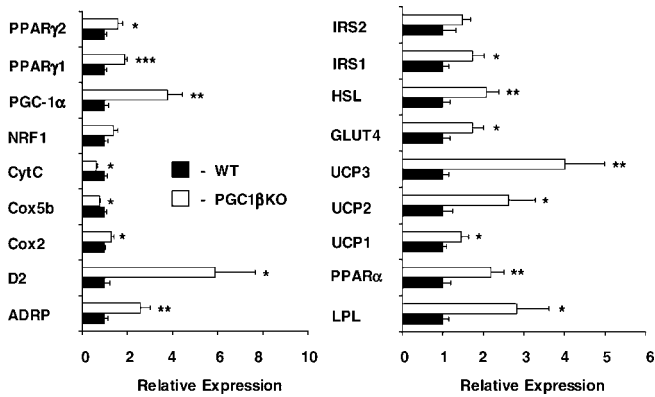


Figure 3. PGC-1 β Ablation Results in Major Changes in BAT Metabolic Gene Expression

Expression levels of mRNA were assessed on interscapular BAT from 12-wk-old male WT (black bars) and PGC1 β KO (white bars) mice. Individual measurements are standardized using 18S, and the average of the WT group set to 1. $n = 5-7$ mice per group. DOI: 10.1371/journal.pbio.0040369.g003

Ablation of PGC-1 β did not result in differences in basal levels of plasma glucose or insulin. Similarly, glucose tolerance tests and insulin tolerance tests (GTTs and ITTs, respectively) performed on 16-wk male and female mice either on chow or after a 13-wk HFD did not reveal differences among genotypes (Figure S3). Therefore, the PGC1 β KO mouse is leaner, has increased energy expenditure, and remains insulin sensitive.

Reduced Expression of ETC Components Despite Increased PGC-1 α mRNA Expression in the BAT of PGC1 β KO mice

Examination of BAT in chow-fed 12-wk-old PGC1 β KO male mice and WT littermates showed major changes in the expression of genes involved in intermediary metabolism (Figure 3). At ambient temperature, we identified a 4-fold compensatory increase in the expression of PGC-1 α when PGC-1 β was ablated. We also observed a 5.9-fold elevation in the thyroid-dependent pro-thermogenic enzyme *D2-deiodinase*. These changes were associated with up-regulation in PGC1 β KO mice of genes involved in glucose and fatty acid metabolism (including *GLUT4*, *PPAR α* , *ADRP*, *LPL*, and *HSL*) as well as elevations in PPAR γ 1 and 2 and all three UCP isoforms. These changes suggested that increased PGC-1 α expression was overcompensating for a lack of PGC-1 β . Despite this up-regulation of PGC-1 α , ablation of PGC-1 β still resulted in a specific decreased expression of genes involved in mitochondrial ETC such as *Cox5b* and *CytC*. In addition, a further range of mitochondrially encoded (Figure 4A) and nuclear-encoded (Figure 4B) ETC mRNAs were also reduced in PGC1 β KO mouse BAT. The mitochondrially encoded *Cox2* was the only ETC subunit measured in PGC1 β KO BAT with increased expression. Western blotting analysis of ETC components in BAT lysates from 15-wk-old female mice revealed decreases in subunits from complexes I to IV in PGC1 β KO mice (Figure 4C). Similarly, assessment of succinate dehydrogenase subunit B (SDHB, complex II) and *Cox4* protein levels in isolated mitochondrial preparations were both reduced in PGC1 β KO mice (Figure 4D). ATP synthase subunit β was unchanged. Taken together, these results

demonstrate defective ETC expression and protein composition in the BAT of PGC1 β KO mice, which cannot be fully compensated for by up-regulation of PGC-1 α . Despite these defective changes, mitochondrial volume fraction was only marginally affected in BAT of PGC1 β KO mice (Figure 4E, WT versus PGC1 β KO: $5.0 \pm 0.3\%$ versus $4.4 \pm 0.2\%$, $n = 4$ mice per group, $p =$ not significant [NS]) and there was no difference in BAT lipid content as determined by light microscopy (WT versus PGC1 β KO: 13.7 ± 0.8 versus 13.1 ± 0.9 , $n = 4$ mice per group, $p =$ NS). This suggests that the up-regulation of PGC-1 α in BAT can compensate some, but not all, aspects of the mitochondrial system in this tissue.

PGC1 β KO Mice Are Cold-Tolerant but Display Abnormal Responses to Norepinephrine-Induced Energy Expenditure

A stepwise acclimatisation to cold exposure (4 °C) and towards thermoneutrality (30 °C) was performed on male mice that were 16 wk old at the end of the 3-wk cold-acclimatisation process. The rationale for these experiments was to identify the contribution of PGC-1 β to energy expenditure in these two directly opposing thermogenic scenarios. PGC1 β KO mice survived at 4 °C after this acclimatisation process. BAT pad weight was similarly increased by cold-acclimatisation in both WT (BAT weight in mg for 30 °C versus 4 °C: WT 117.8 ± 7.1 versus 145.5 ± 9.4 , $p < 0.05$, $n = 5$ mice per group) and PGC1 β KO mice (107.9 ± 9.1 versus 160.0 ± 10.3 , $p < 0.01$, $n = 4$ mice per group), without differences in BAT weight between the genotypes in either condition. Cold-acclimatised PGC1 β KO mice had decreased basal metabolic rate compared to WT (Figure 5A) and had a higher RER than WT mice, suggesting that PGC1 β -deficient adaptation to cold exposure may involve preferential use of carbohydrates (Figure 5B). Thermoneutrality studies showed that contrary to the increased resting metabolic rate observed at ambient temperature, when PGC1 β KO mice are housed and measured at thermoneutrality, they have reduced basal metabolic rate compared to WT (Figure 5A). Of note, PGC-1 α up-regulation observed in PGC1 β KO mice at ambient temperature was prevented at thermoneutrality (see below).

To test the maximal BAT-based nonshivering thermogenesis capacity, we used a norepinephrine (NE) challenge (Figure 5C). Whereas NE provoked the expected large (almost 4-fold) increase in O₂ consumption in cold-adapted WT mice, the same stimulus in cold-adapted PGC1 β KO mice only reached 60% of the WT response. (Figure 5C). NE administration to mice kept at thermoneutrality revealed that whereas WT mice exhibited a physiological small increase in O₂ consumption after being given NE, O₂ consumption in the PGC1 β KO mice housed at thermoneutrality was essentially unaffected by NE. This demonstrates that the ability of the BAT to mediate thermoregulatory thermogenesis after a period of cold acclimatisation or during thermoneutrality is blunted by the absence of PGC-1 β .

Gene expression of BAT from cold-acclimatised and thermoneutrally maintained mice was analysed. Comparison of gene expression patterns between WT and PGC1 β KO mice housed at 30 °C (Figure 5D) revealed the same differences between the genotypes as previously seen in mice housed at ambient temperatures (Figure 3). In addition, many of the genes examined concerning fuel handling (e.g., *SREBP1c*,

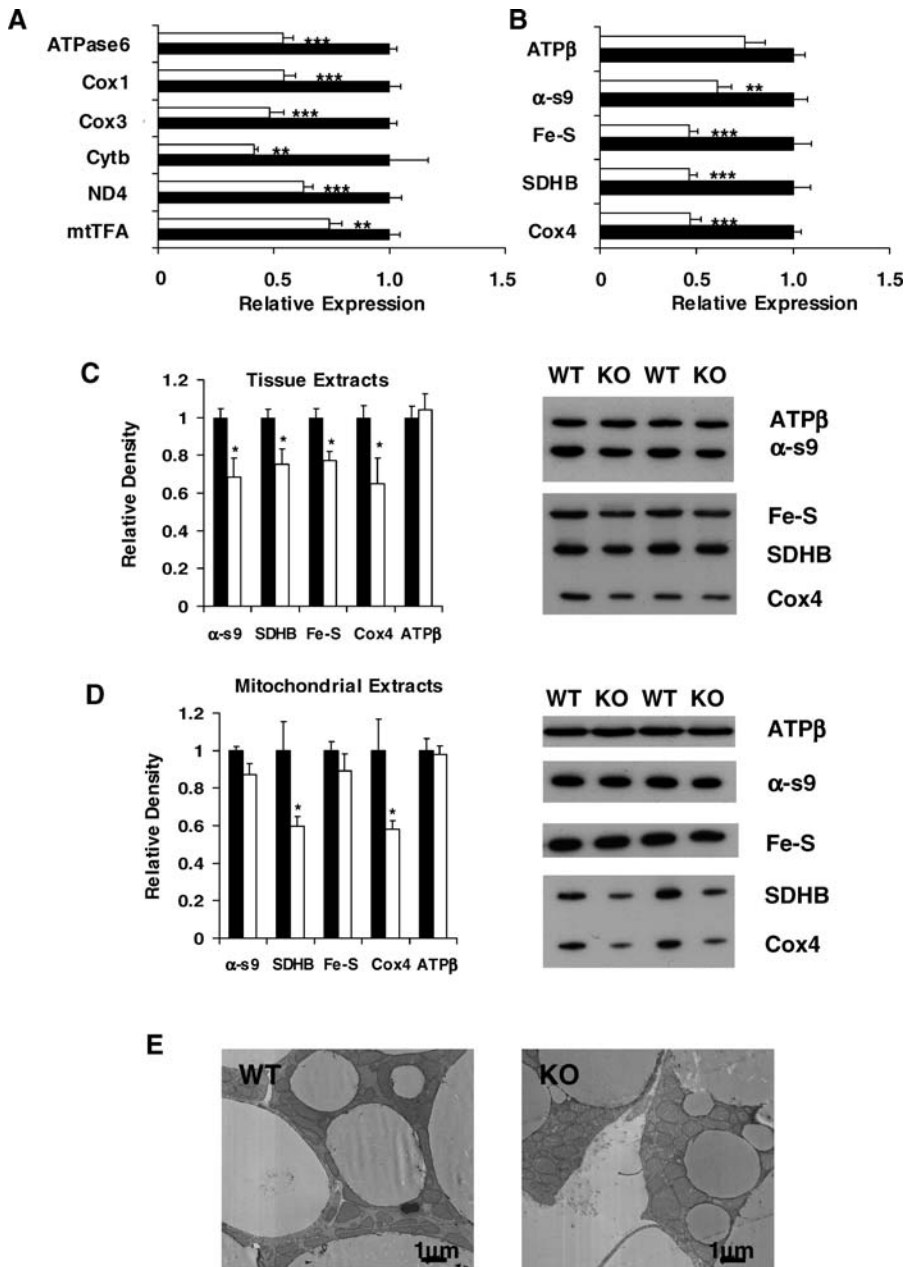


Figure 4. PGC-1 β Ablation Reduces ETC Gene and Protein Expression but Mitochondrial Volume Fraction is Unaffected

(A and B) Expression levels of (A) nuclear-encoded and (B) mitochondrially encoded genes were assessed on interscapular BAT from 12-wk-old male WT (black bars) and PGC1 β KO (white bars) mice. Individual measurements are standardized using 18S, and the average of the WT group set to 1. $n = 5-7$ mice per group.

(C and D) BAT protein levels of ETC and OxPhos components from 15-wk-old female mice were assessed by western blotting of samples from (C) tissues and (D) mitochondrial fractions. WT, black bars and PGC1 β KO, white bars. Complex I, α -subcomplex 9 (α -s9); complex II, succinate dehydrogenase subunit B (SDHB); complex III, Fe-S core protein (Fe-S); complex IV, Cox4; complex V, ATP synthase subunit β (ATP β). $n = 5-6$ mice for each protein, with the average value of the WT group set to 1. Representative blots showing two samples from each genotype.

(E) Representative electron micrographs from BAT of WT (left panel) and PGC1 β KO (right panel) mice.

DOI: 10.1371/journal.pbio.0040369.g004

GLUT4, *LPL*, *PPAR γ*) were similar in cold-acclimated WT and PGC1 β KO mice (Figure 5D, left panel). However, cold-acclimated PGC1 β KO BAT still had decreased expression of the ETC genes *Cox4*, *Cox5b*, and *CytC* (Figure 5D, right panel). Similarly, there was significantly lower expression of UCP1 and MCAD in cold-acclimated PGC1 β KO BAT than in WT. With cold exposure, PGC-1 α mRNA was increased to a similar extent in both WT and PGC1 β KO mice, and PGC-1 β expression was increased in WT mice. Also, as indicated

above, there was no difference in PGC-1 α expression between the genotypes at thermoneutrality. As expected, cold acclimation increased levels of UCP1 protein in WT (total interscapular BAT UCP1 protein 30 °C versus 4 °C, standardised to WT 4 °C: 12.9 ± 2.8 versus 100.0 ± 7.4 ; $n = 5$ mice per group) and also in PGC1 β KO mice (14.9 ± 2.9 versus 140.9 ± 19.9 ; $n = 4$ mice per group). Total BAT UCP1 protein was near-significantly elevated ($p = 0.07$) in cold-acclimated PGC1 β KO mice compared to cold-acclimated WT mice.

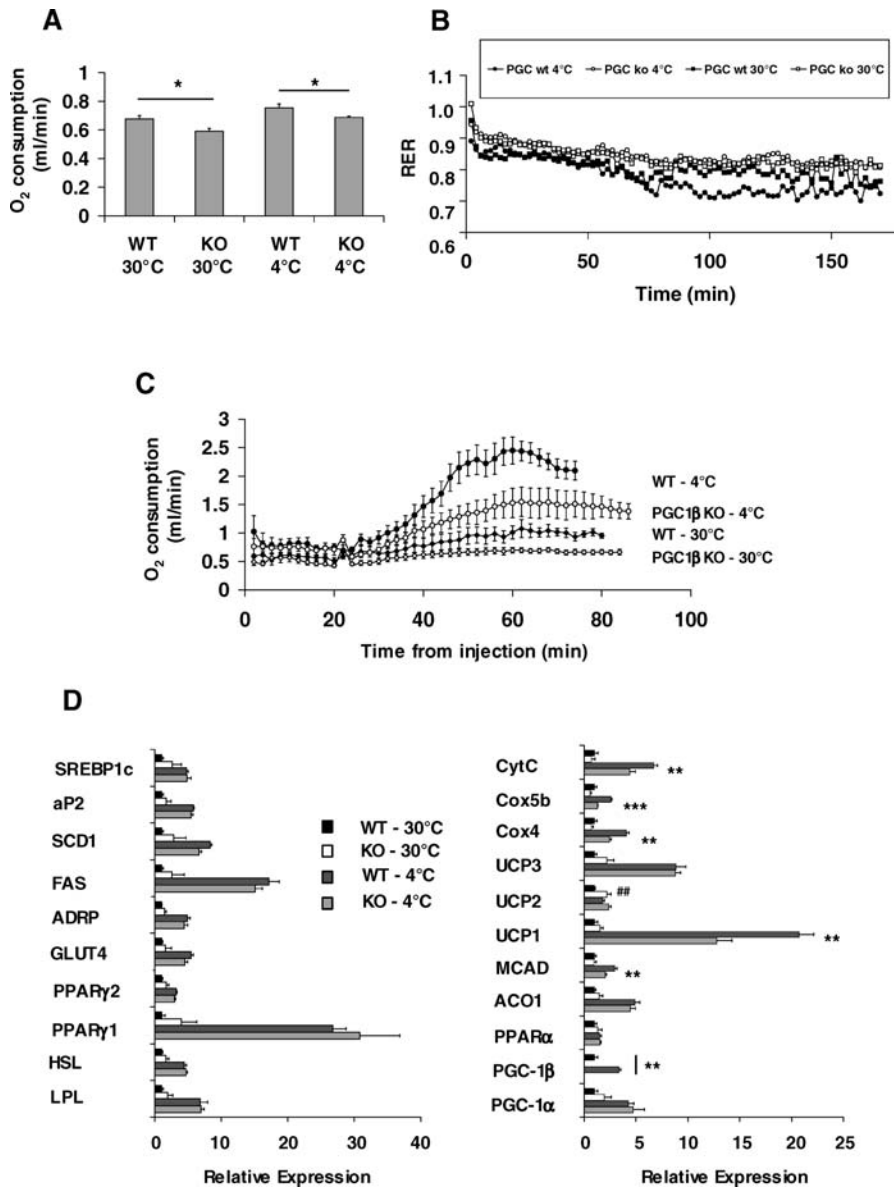


Figure 5. Thermoneutral and Cold-Adapted PGC1 β KO Mice Display Reduced Resting and NE-Stimulated Energy Expenditure

Male WT and PGC1 β KO mice were acclimatised to 30 °C or 4 °C as stated in the Materials and Methods.

(A) Oxygen consumption per mouse (ml/min). Similar results were obtained when the data were standardised using the body weight (kg)^{0.75} scaling; WT, black bars; PGC1 β KO, white bars.

(B) RER. Solid circles, WT at 4 °C; open circles, PGC1 β KO at 4 °C; solid squares, WT at 30 °C; open squares, PGC1 β KO at 30 °C.

(C) Oxygen consumption per mouse (ml/min) measured post-administration of 1 mg/kg norepinephrine.

(D) BAT mRNA expression in thermoneutral and cold-adapted mice. WT thermoneutral, black bars; PGC1 β KO thermoneutral, white bars; WT cold-adapted, dark gray bars; PGC1 β KO cold-adapted, light gray bars. Individual measurements are standardized using 36B4 and the average of the WT, thermoneutral group was set to 1. $n = 4-5$ mice per genotype per condition for each experiment. * indicate a significant difference between cold-adapted WT and PGC1 β KO mice. ## indicates a significant difference between thermoneutral WT and PGC1 β KO mice.

DOI: 10.1371/journal.pbio.0040369.g005

Thus, the inhibition of cold-acclimatised BAT activity in PGC1 β KO mice occurs as a result of reduced ETC expression, despite otherwise normal BAT recruitment and UCP1 protein expression.

Gene Expression Pathway Analysis in PGC1 β KO Tissues Shows Global Impairment in Mitochondrial Function and Substrate Use

Binomial pathway enrichment analysis using pathways from the Kyoto Encyclopedia Genes and Genomes (KEGG) was performed on gene expression from spotted arrays

generated from BAT of PGC1 β KO and WT mice to identify alterations in whole genetic pathways (Table 2). Down-regulated KEGG pathways include OxPhos, ubiquinone biosynthesis, and ATP synthesis. In addition, we saw decreases in glycolysis/gluconeogenesis, the citric acid cycle, and many of the amino acid metabolism pathways that feed substrates into these systems. Only purine metabolism and glycerolipid metabolism pathways were significantly up-regulated in BAT. A full list of altered KEGG pathways can be found in Dataset S1. Similar gene expression pathway analysis was also performed in liver and heart tissues. We identified only two

Table 2. Major KEGG Pathways Are Changed in PGC1 β KO Mouse BAT

Pathway Type	Pathway Name	<i>p</i> Value
DOWN	Oxidative phosphorylation	0.000
	Citrate cycle (TCA cycle)	0.000
	ATP synthesis	0.001
	Pyruvate metabolism	0.015
	Galactose metabolism	0.002
	Cysteine metabolism	0.001
	Reductive carboxylate cycle (CO ₂ fixation)	0.000
	Tyrosine metabolism	0.002
	Ubiquinone biosynthesis	0.001
	Glycolysis gluconeogenesis	0.004
	Phenylalanine metabolism	0.001
	Arginine and proline metabolism	0.004
	Starch and sucrose metabolism	0.001
	Phenylalanine tyrosine and tryptophan biosynthesis	0.003
	UP	Glycerolipid metabolism
Purine metabolism		0.046

RNA was isolated from 14-wk-old normal diet-fed male PGC1 β KO and WT mice and then analysed using spotted arrays as described in the Materials and Methods. Data are displayed as pathway name followed by *p* value for the binomial test. A pathway *p* value of <0.05 was considered significant.

DOI: 10.1371/journal.pbio.0040369.t002

KEGG pathways, OxPhos, and ATP synthesis that were decreased in all three tissues—BAT, heart, and liver (Table S3). This suggests a global role for PGC-1 β in the maintenance of normal gene expression encoding for mitochondrial proteins.

Tissue Mitochondrial Activity, but Not Isolated Mitochondrial Function, Is Impaired in PGC1 β KO Soleus Muscle

We assessed whether reduced expression of ETC genes were associated with functional defects in permeabilised soleus muscle fibres (Figure 6). Both state 3 and state 4 mitochondrial respiration were reduced in PGC1 β KO fibres, suggesting reduced electron chain capacity and OxPhos activity (Figure 6A). There was no change in the respiratory control ratio (RCR; state 3/state 4), suggesting that the differences between WT and PGC1 β KO mice were not related to intrinsic differences in mitochondria function but to reduced numbers of mitochondria per fibre. In agreement with this, ATP synthesis was decreased in PGC1 β KO fibres (Figure 6B), and a trend for decreased ATP/O ratio in PGC1 β KO muscle fibres was also observed (Figure 6C). This suggested that PGC1 β KO soleus fibres not only produce less ATP than WT fibres did, but they were also less efficient at converting reduced substrate into ATP. Gene expression analysis of 12-wk-old male soleus muscles demonstrated that PGC1 β KO mice have reduced ETC expression (*Cox4* and *Cox5b*), which corresponds to reduced soleus mitochondrial capacity (Figure S4). These results were supported by a decreased mitochondrial volume fraction in the soleus of PGC1 β KO mice performed by stereological analysis (WT versus PGC1 β KO: 20.4 \pm 0.7% versus 16.8 \pm 0.8%, *p* = 0.012) (Figure 6D).

To assess whether this oxidative defect could be attributed to the functionality of individual mitochondria, we measured oxidative activity of isolated soleus mitochondria. In all states

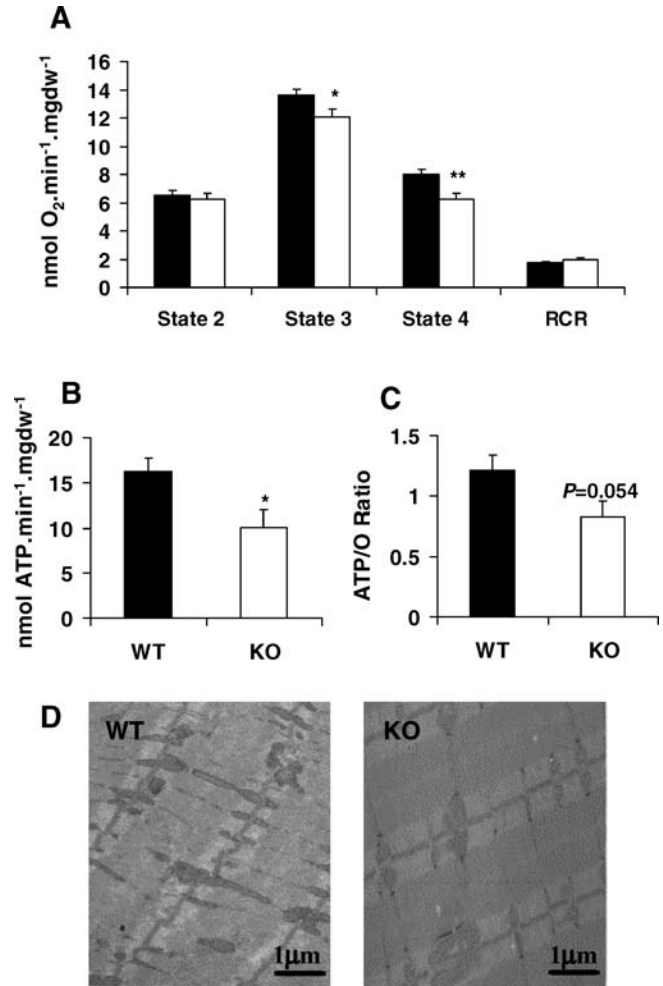


Figure 6. Isolated Soleus Fibres from PGC1 β KO Mice Have Reduced Mitochondrial Activity

Soleus fibres were isolated from WT (black bars) and PGC1 β KO mice (white bars) and permeabilised to allow measurement of tissue-associated mitochondrial function.

(A) Mitochondrial respiratory parameters for state 2 (V_0), state 3 (V_{ADP}), state 4 ($V_{oligomycin}$), and respiratory control ratio (RC).

(B) ATP synthesis rates in permeabilised soleus fibres.

(C) ATP/O ratio in permeabilised soleus fibres. Data are standardised to mg of muscle dry weight (mgdw). *n* = 9 WT mice, 11 PGC1 β KO mice.

(D) A representative electron micrograph of soleus muscle from WT (left panel) and PGC1 β KO (right panel) mice.

DOI: 10.1371/journal.pbio.0040369.g006

examined, there was no significant difference between WT and PGC1 β KO-derived soleus mitochondria (Figure S5). In addition, no differences amongst genotypes were observed when RCR (Figure S5B) or proton leak were measured (Figure S5C).

PGC-1 β Ablation Reduces Mitochondrial Content of the Heart and Blunts the Effect of Adrenergic Stimulation on Heart Rate

We hypothesized that defective PGC-1 β may result in electromechanical myocardial dysfunction in the hearts of PGC1 β KO mouse. Heart weights from PGC1 β KO mice were similar to WT in chow-fed 14-wk-old male mice (Table S2). In addition, under basal conditions, PGC1 β KO hearts showed no histological abnormalities compatible with fibrosis or

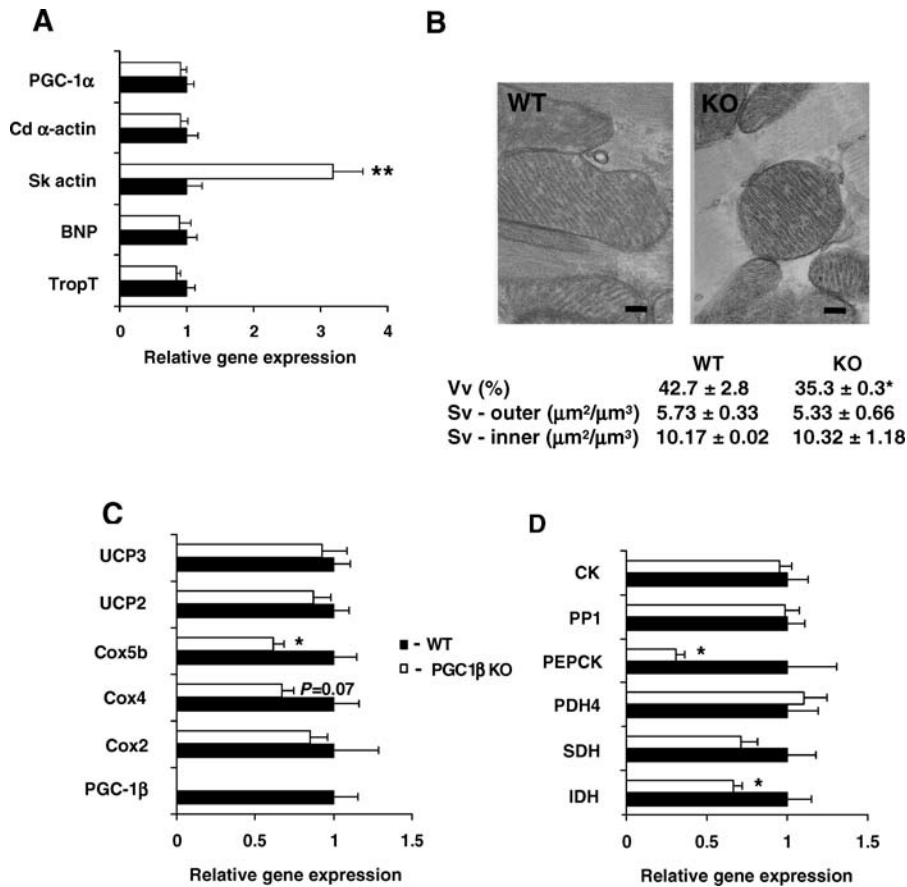


Figure 7. Alterations in Gene Expression and Mitochondrial Dimensions in Hearts of PGC1 β KO Mice

(A) Expression levels of mRNA were assessed on hearts from 24-wk-old male WT (black bars) and PGC1 β KO (white bars) mice. Individual measurements are standardized using 18S, and the average of the WT group set to 1. $n = 5-7$ mice per group.

(B) A representative electron micrograph of mitochondria from WT (left panel) and PGC1 β KO (right panel) hearts. The bar indicates a measurement of 200 nm.

(C) mRNA expression of key genes for mitochondrial function in 24-wk-old WT and PGC1 β KO mouse hearts.

(D) mRNA expression of key genes for metabolic function in 24-wk-old male WT and PGC1 β KO mouse hearts.

DOI: 10.1371/journal.pbio.0040369.g007

inflammatory infiltrates (unpublished data). The expression of molecular markers of cardiac hypertrophy, such as α -actin, natriuretic peptide precursor type B, or troponin I, were all normal in 24-wk-old male PGC1 β KO hearts (Figure 7A). The only transcriptional change that can be associated with myocardial dysfunction was the up-regulation of skeletal muscle actin in PGC1 β KO compared with WT mice. PGC-1 α mRNA expression was also unchanged in PGC1 β KO hearts. PGC1 β KO hearts had a decreased mitochondrial volume fraction as indicated by stereological analysis (42.8 \pm 2.8 % versus 35.3 \pm 0.3 %, $p = 0.05$; Figure 7B). Despite this result, PGC1 β KO and WT heart mitochondria were similarly packed between myofibres, and there were no changes in cristae surface density, S_v (per unit volume of mitochondria). This suggests that the internal structure of the mitochondria was normal in the PGC1 β KO hearts. In agreement with the gene expression pathway analysis, the expression of *Cox4* ($p = 0.07$) and *Cox5b* was down-regulated in heart of 14-wk-old PGC1 β KO compared with WT mice, whereas *Cox2* expression was unchanged (Figure 7C).

Male, 26-wk-old PGC1 β KO and WT littermates were challenged with acute infusion of the β_1 , α_1 -adrenergic selective agonist dobutamine. Haemodynamic recordings

showed that baseline heart rate and left ventricular contractility (+dP/dt or -dP/dt) were similar between genotypes. As expected during infusion of 10 ng dobutamine per min per g body weight (ng/min/g BW), WT mice increased their heart rate, an effect that was blunted in PGC1 β KO mice (Figure 8A). This inability to increase heart rate was even more evident using a 40 ng/min/g BW dobutamine infusion ($p < 0.05$ for 8, 10, and 12 min post-injections). Ventricular performance during the dobutamine challenge was the same in WT and PGC1 β KO mice (Figure 8B and 8C).

PGC-1 β Modulates the Response of the Liver to an Acute HFD Challenge

Gene expression analysis of fed-state 12-wk-old male mouse livers showed ablation of PGC-1 β but did not result in major changes in mRNA expression levels (Figure S6). Only *Cox4* was decreased in the PGC1 β KO livers, a result that was in agreement with gene expression pathway analysis (Table S3). When 8-wk-old female PGC1 β KO mice were challenged with a 24-h period of Surwit HFD, liver mass increased as a proportion of body weight (Figure 9A). This effect was not observed in WT mice fed the same diet. Histological analysis revealed that PGC1 β KO mice fed the Surwit diet developed severe hepatic steatosis compared to WT mice (Figure 9B).

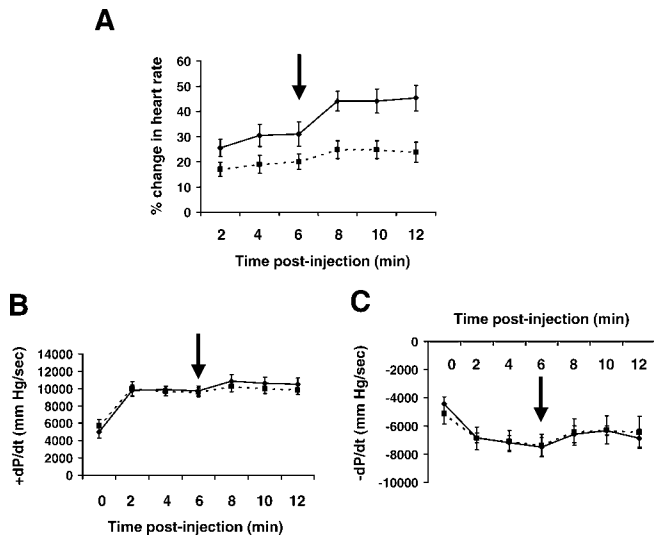


Figure 8. PGC1 β KO Hearts Display a Blunted Heart Rate Response to Dobutamine Stimulation In Vivo

PGC1 β KO and WT littermates (male, 26-wk-old) were treated as stated in Material and Methods and infused with 10 or 40 ng/min/g BW dobutamine to measure in vivo hemodynamic responses WT, solid line; KO, dashed line.

(A) Percentage change in heart rate from basal during dobutamine infusion.

(B and C) Measurement of ventricular performance, dP/dt , during infusion. The arrow marks the increase in dobutamine concentration in the infusion from 10 to 40 ng/min/g BW. $n = 5$ mice per genotype.

DOI: 10.1371/journal.pbio.0040369.g008

Increased fat deposition in PGC1 β KO livers was associated with normal plasma non-esterified fatty acids (NEFA) levels (Table 3). As expected, plasma triglyceride levels increased in WT mice in response to 24-h HFD, however plasma triglyceride levels were significantly lower in PGC1 β KO than WT mice when fed the Surwit diet. When compared to WT mice, the PGC1 β KO mice had lower basal levels of high-density lipoprotein (HDL) and LDL-associated cholesterol and elevated VLDL-associated cholesterol. Administration of a fat-enriched diet increased the amount of cholesterol associated with VLDL, HDL, and LDL particles in WT mice (Table 3). However, PGC1 β KO mice had inappropriately low levels of VLDL and blunted increases on total cholesterol and HDL- and LDL-associated cholesterol in plasma. Thus, defective PGC-1 β results in lipid accumulation in liver and decreased circulating triglyceride-rich VLDL lipoproteins following a high-dietary lipid load.

Of interest and contrary to previous reports, we were unable to detect increases in PGC-1 α and PGC-1 β mRNAs in response to acute HFD in WT liver (Figure S7). We observed that *SCD-1* and *HMG-CoA reductase* were significantly elevated in WT livers in response to Surwit diet compared to chow WT controls and that similar changes were not observed in PGC1 β KO mouse livers after the Surwit diet (Figure S7).

Discussion

Accumulating evidence indicated that PGC-1 β may play a role in energy homeostasis through its effects on substrate metabolism and mitochondrial activity [4,6,7,13–15,19]. However, the function and relevance of PGC-1 β in the control of whole-organism energy metabolism is not well

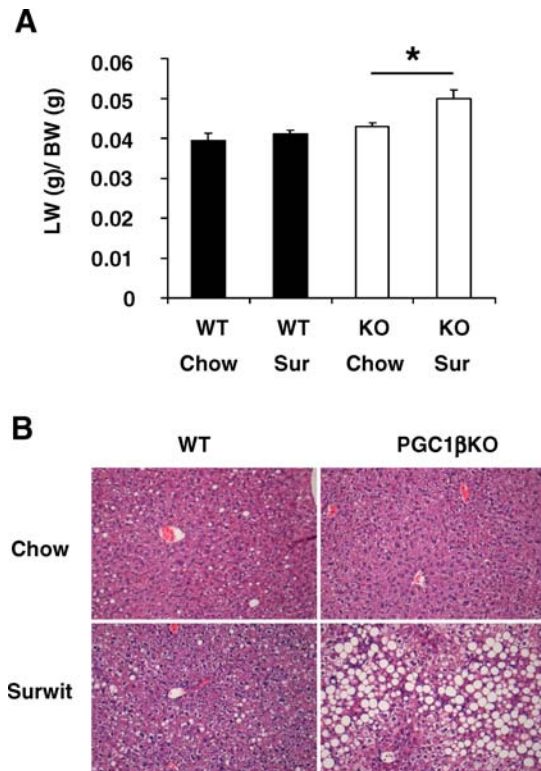


Figure 9. PGC1 β KO Mice Demonstrate Increased Liver Mass and Development of Fatty Liver after 24 h HFD

Female 8-wk-old mice were given normal chow or Surwit HFD (Sur) for 24 h. Tissues were then collected for analysis.

(A) Liver weight, as standardized by body weight (LW/BW) for WT (black bars) and PGC1 β KO (white bars) after 24 h diets.

(B) Representative histological sections from mice given normal or Surwit diet for 24 h. $n = 6$ –7 mice per group.

DOI: 10.1371/journal.pbio.0040369.g009

defined. To address this question, we generated and phenotyped a PGC1 β KO mouse model. The PGC1 β KO mouse is viable and apparently healthy. However, using a phenotyping strategy that combines physiological stress challenges guided by information obtained from a systems biology approach, we found that PGC1 β KO mice have a general defect in mitochondrial function, a defect that is partly compensated for by mechanisms that are usually involved in adaptation to increased energy demands, such as up-regulation of PGC-1 α .

The effect of PGC-1 β controlling mitochondrial activity was investigated at the mRNA level using spotted array technology and bioinformatics pathway analysis. This approach showed that deletion of PGC-1 β results in a significant mitochondrial phenotype. Multi-tissue comparisons demonstrated that PGC-1 β controls the level of expression of ETC and OxPhos genes across all the organs studied and that this defect can only be partially compensated for in BAT and WAT by up-regulation of PGC-1 α . However, the decrease in mRNA expression of ETC components is not necessarily seen at the protein level. These data suggest that although PGC-1 β may be a controller of mitochondrial gene expression, in the absence of PGC-1 β , additional factors such as protein degradation may be counter-regulated in specific tissues in an attempt to normalise levels of mitochondrial activity.

Our initial hypothesis was that dysregulation of ETC gene

Table 3. Serum Lipid Biochemistry from 24-h Surwit Diet-Fed WT and PGC1 β KO Mice

Lipid	WT - Chow	WT - Surwit	PGC1 β KO - Chow	PGC1 β KO - Surwit
Triglycerides (mM)	0.39 \pm 0.03 ^a	0.66 \pm 0.12 ^{a,b}	0.21 \pm 0.04	0.35 \pm 0.03 ^b
NEFA (mM)	0.64 \pm 0.05	0.82 \pm 0.12	0.60 \pm 0.05	0.71 \pm 0.07
Cholesterol (mM)	3.34 \pm 0.20 ^{a,b}	5.37 \pm 0.24 ^{a,c}	2.20 \pm 0.23 ^{b,d}	3.45 \pm 0.30 ^{c,d}
VLDL (mM)	0.026	0.049	0.037	0.025
HDL (mM)	0.29	0.46	0.23	0.35
LDL (mM)	3.06	4.86	1.93	3.07

Female WT and PGC1 β KO mice were placed on Surwit diet for 24 h or maintained on normal diet. At the end of the time period, the mice were sacrificed and blood serum analysed. $n = 5-7$ mice per condition. For cholesterol-associated lipoproteins, serum samples for each group were pooled and analysed.

^aSignificant comparisons between groups.

^bSignificant comparisons between groups.

^cSignificant comparisons between groups.

^dSignificant comparisons between groups.

DOI: 10.1371/journal.pbio.0040369.t003

expression would increase the likelihood that the PGC1 β KO mouse would become obese. However, despite its mitochondrial phenotype, the PGC1 β KO mouse showed elevated resting metabolic rate and lower body weight compared to wild type littermates under ambient room temperature conditions. This phenotype is possibly due to the compensatory increase in expression of PGC-1 α and its target genes in BAT. The increase in BAT PGC-1 α expression may cause the higher degree of energy expenditure and relatively conserved mitochondria volume fraction despite reductions in ETC gene and protein expression. PGC-1 α was also up-regulated in PGC-1 β -deficient WAT, but its induction was not robust enough to produce a BAT-like histology or induction of typical BAT genes. Instead, within the reduced WAT content of the PGC1 β KO mice, there was a greater proportion of larger, hypertrophic adipocytes. This result suggests that PGC-1 β may play an as yet unknown role in white adipocyte biology, and the nature of this role requires further investigation.

Of interest, despite marked elevation of PGC-1 α levels in PGC1 β KO BAT, we did not observe a full restoration of the expression of mitochondrial genes back to WT levels. However, unlike the heart or skeletal muscle, organs where PGC-1 α was not up-regulated, the mitochondrial fraction of BAT tissue was preserved in PGC1 β KO mice. Thus, there may be partial functional overlap between PGC-1 α and PGC-1 β , concerning mitochondrial structure and function, which allows the development of an appropriate mitochondrial BAT content but fails to correct deficiencies in ETC composition. BAT was the only tissue out of three metabolically relevant tissues examined using electron microscopy that displayed relatively normal mitochondrial fraction, suggesting that further tissue function-specific mechanisms may be able to correct for PGC-1 β ablation. However, the BAT gene expression pattern in PGC1 β KO mice also showed altered expression of genes involved in intermediary metabolism, a pattern of gene expression that may also be primarily the result of PGC-1 α up-regulation. Our conclusion from these gene expression analyses is that whereas PGC-1 β may be required to set the basal level of mitochondrial ETC gene expression, it is not essential for normal expression of metabolic pathways such as glycolysis, the citric acid cycle, and fatty acid oxidation.

We hypothesized that the elevated resting metabolic rate

seen in ambient-temperature housed PGC1 β KO mice may be reversed under conditions of thermoneutrality, particularly if it was caused by compensatory up-regulation of PGC-1 α . Under thermoneutral conditions, levels of PGC-1 α gene expression are suppressed in BAT in response to the lower thermogenic and therefore oxidative demands of life at 30 °C. At thermoneutral conditions, PGC-1 α mRNA expression was equivalent in WT and PGC1 β KO BAT. Interestingly, under thermoneutral conditions, the PGC1 β KO mouse exhibited reduced basal metabolic rate compared to the WT mouse. The energy expenditure measurements with mice acclimatised to 4 °C and 30 °C were performed at 33 °C. This measurement at thermoneutrality gives an indication of the basal metabolic rate. Under these experimental conditions, we can conclude that the PGC1 β KO mouse has a reduced basal metabolic rate. The data from mice housed in ambient (22 °C) conditions were also generated at ambient conditions (Table 1). Therefore, this measurement represents energy expenditure in “normal” environmental conditions, when the body weights of the PGC1 β KO mice are lower than WT. Under these experimental conditions, this measurement is composed of both basal metabolic rate and any additional metabolic effort required to maintain body temperature in this suboptimal thermal environment. Given that basal metabolic rate is reduced in 30 °C- and 4 °C-acclimatised PGC1 β KO mice, it could be assumed that at ambient temperatures, basal metabolic rate is also reduced, but that the metabolic adaptation required for body temperature defense is actually greater in the PGC1 β KO mouse. This suggests that PGC-1 β may contribute to BAT thermogenesis in states of low metabolic demand (as is the case for BAT at 30 °C), whereas induction of PGC-1 α regulates BAT thermogenesis as environmental temperatures fall.

It has been suggested that PGC-1 β plays a role in BAT accumulation and function during cold exposure [6]. PGC1 β KO mice tolerated cold acclimatisation, despite the fact that under these conditions, PGC1 β KO mice had decreased ETC gene expression and had decreased maximal thermogenic capacity in BAT, as shown by the lower oxygen consumption rate in response to adrenergic stimulation. Both WT and PGC1 β KO mice up-regulated PGC-1 α to a similar extent under conditions of cold exposure, suggesting that there is a maximal capacity of PGC-1 α up-regulation in BAT. Alternatively, survival in cold may also be facilitated by

the ability of the mice to maintain some fraction of increased metabolic activity through continued shivering [22–24]. Therefore, although the total metabolic capacity provided by PGC-1 α in cold-exposed PGC1 β KO mice was sufficient for their survival, our results indicate that PGC-1 β regulates a large fraction of the thermogenic capacity of the BAT tissue.

Studies focused in other metabolically relevant organs where PGC-1 β is well expressed also indicated that ablation of PGC-1 β resulted in impaired metabolic capacity. For example, mitochondrial volume fraction in soleus of PGC1 β KO mice was decreased, and permeabilised soleus muscle fibres from PGC1 β KO mice had reduced oxygen consumption and ATP synthesis compared to WT-derived fibres. Similar experiments using isolated soleus mitochondria from PGC1 β KO mice failed to show any abnormalities in metabolic performance, indicating that metabolic defects in PGC1 β KO soleus tissue relate to lower mitochondrial density relative to WT, although individual mitochondria retain similar metabolic properties.

The heart is the third oxidative tissue that is a major site of PGC-1 β expression. Absence of PGC-1 β in heart also led to a reduction of mitochondrial fraction, consistent with reduced cardiac expression of ETC genes. However, despite these potential bioenergetic defects, PGC1 β KO mice have normal basal heart rates and ventricular contractility. Left ventricular function was also maintained after dobutamine treatment, suggesting that despite their mitochondrial defect, the PGC-1 β -deficient hearts are able to adapt normally to imposed hemodynamic loads. The only difference in adrenergic stress that we observed between the PGC1 β KO mice and WT was a blunting of the expected increase in heart rate in the PGC1 β KO mice. A similar defect in heart rate regulation was also found in the PGC-1 α knockout mice [14], suggesting that both PGC-1 α and PGC-1 β may have a direct effect in controlling the activity of heart pacemakers. Overall, our results indicate that ablation of PGC-1 β impairs heart mitochondrial function but that this defect is not severe enough to induce heart failure. However, a more chronic intervention study would be required to establish the relative importance of these PGC isoforms in cardiac energy supply and control.

To this point, we have discussed exclusively a role for PGC-1 β in oxidative metabolism. Nonetheless, PGC-1 β may also play an important role in regulating hepatic lipid production [11,17]. Contrary to previous reports, we did not observe either PGC-1 β induction after 24-h HFD in the liver of our control mice or differences in *FAS* and *SREBP1c* gene expression between controls and PGC1 β KO mice. However, we did observe a reduction in circulating total cholesterol and alterations in the lipoprotein-associated cholesterol pattern in chow-fed conditions. Feeding for 24 h with a saturated fat-enriched HFD was associated with severe hepatic lipid accumulation and decreased total triglycerides, cholesterol, and VLDL and LDL-cholesterol plasma levels in PGC1 β KO mice compared to WT. These results agree with a recent report suggesting that PGC-1 β is a likely mediator of VLDL secretion by acting via interactions with *Foxa2* to alter microsomal transfer protein expression [17]. However, it is also possible that PGC-1 β is necessary for additional aspects of hepatic lipid handling, including modification of lipid storage pathways and for controlling the balance between fatty acid synthesis and oxidation. Indeed, our pathway

analysis suggests that the ETC in liver is expressed at a lower level and this may contribute to the steatosis after acute HFD treatment.

Our results indicate that PGC-1 β has a well-defined role in controlling mitochondrial gene expression and function in many different organs. Despite this, PGC-1 β can be ablated without overt metabolic failure, at least in unstressed conditions. This may be due in part to robust compensatory mechanisms, as demonstrated by the up-regulation of PGC-1 α expression in WAT and BAT. Interestingly, other organs such as liver, muscle, or heart did not show up-regulation of PGC-1 α under the conditions investigated. Following from these differences in PGC-1 α expression, it is likely that the lean phenotype of this mouse model at ambient temperature should be considered the result of overcompensation mediated by up-regulation of PGC-1 α , at least in BAT and WAT. Conversely, defects observed in skeletal muscle, heart, and liver are more likely to be the result of the absence of PGC-1 β given the lack of PGC-1 α induction in those tissues. When considering the roles played by PGC-1 α and PGC-1 β , our results show that there are specific effects of PGC-1 β that cannot be compensated for by PGC-1 α . Taken altogether, our results indicate that PGC-1 β seems to cover basal bioenergetic needs whereas PGC-1 α provides the extra bioenergetic support required under conditions of increased energy demand.

Materials and Methods

Materials and reagents. All reagents used in this paper were supplied from Sigma-Aldrich (St. Louis, Missouri, United States), unless stated.

Animal care. Animals were housed in a temperature-controlled room with a 12-h light/dark cycle. Food and water were available ad libitum unless noted. All animal protocols used in this study were approved by the UK Home Office, The Institutional Animal Care and Use Committee of the University of Utah, United States, and the Animal Ethics Committees of Gothenburg and North Stockholm, Sweden. Mice were cared for according to the Guiding Principles for Research Involving Animals and Human Beings.

Generation of PGC1 β KO mice. A triple LoxP strategy was used to target the PGC-1 β locus in order to generate mice with both standard and conditional KO alleles at this locus. The targeting vector was a ~8 kilobase (kb) 129/SvJ mouse genomic subclone containing a floxed neomycin phosphotransferase selectable marker cassette inserted into intron 3 and a single LoxP site inserted into intron 5 (Figure 1A). The targeting construct was electroporated into R1 ES cells, and neomycin-resistant clones were selected in G-418-containing media. The clone was injected into C57Bl/6 blastocysts and chimeric males were crossed to C57Bl/6 females. Heterozygous triple LoxP mice were then bred to ROSA26Cre [25] mice in order to generate heterozygous PGC-1 β KO mice which had undergone Cre-mediated deletion of the intervening region of DNA between the outermost LoxP sites. PCR analysis gave a product of approximately 0.5 kb for the Cre-recombined allele and products of approximately 2.8 and 0.6 kb with the WT allele (Figure 1D). Heterozygous PGC-1 β KO mice were then intercrossed to generate mice that were homozygous for the PGC-1 β deletion. Null mutants were verified using RNA prepared from heart and skeletal muscle to demonstrate that exons 4 and 5 had been deleted in the PGC1 β KO mice. Mice used for this research were backcrossed between three and six times to a C57BL6/J background. Littermate controls were used for all experiments. A more complete description for this section can be found in the Protocol S1.

Long-term feeding and growth studies. Mice were placed at weaning (3-wk-old) on normal chow diet (12% fat, 62% carbohydrates, and 26% protein with a total energy content of 12.6 kJ/g) (R3 diet, Lactamin AB, Stockholm, Sweden). Mouse weights were taken at the same time each week, until the end of the specific protocol period. Mice were routinely housed at 22 °C, except for those used for the BAT activity and cold acclimatisation experiments (see below).

Acute dietary measurements and interventions. To examine 48-h food intake, cages (23 \times 16 cm) were prepared with normal chow and incubated at 80 °C for 1 h to correct for any differences in humidity. After 2 h at room temperature, the cages were accurately weighed. 12-h-fasted mice were put in preweighed cages with free access to food and water. After 48 h, the mice were removed and all faecal matter was collected. The cages were reincubated at 80 °C in order to dry out waterspill and urine, and then reweighed after 2 h cooling. The difference in weights of the cage before and after the 48-h assessment produced the weight of food consumed. For measurement of energy content of faeces and food, samples were dried at 55 °C overnight and stored in airtight containers at -20 °C until assayed. The gross energy content of the dried samples was determined using a bomb calorimeter (C5000, IKA Werke GmbH & Co., KG, Germany). To assess the effect of 24-h high-fat feeding, 8-wk-old female mice were assigned into two groups: ad libitum normal food or ad libitum Surwit diet (58% of calories derived from fat, predominantly hydrogenated coconut oil; D12331, Research Diets, New Brunswick, New Jersey, United States). Start of the 24-h period was 9 am. At the end of the time period, mice were killed and dissected as above. Water was freely available during all procedures.

Body composition and indirect calorimetry. For body composition analysis, dual energy x-ray absorptiometry (DEXA, GE Medical Systems Lunar Corporation, Madison, Wisconsin, United States) was performed on isoflurane anaesthetized mice as previously described [26]. Oxygen consumption (VO₂) and carbon dioxide production (VCO₂) were measured using the OxyMax system (Columbus Instruments International, Columbus, Ohio, United States) [27]. Further details can be found in Protocol S1.

GTTs and ITTs on mice fed chow and HFDs were performed as previously described [26].

Cold acclimatisation and BAT activity. PGC1 β KO mice and WT littermates were exposed to 30 °C for 3 wk, placed at 18 °C for 1 wk, and then exposed to 4 °C for 3 wk or kept at 30 °C for the duration of the protocol. For both 30 °C and 4 °C acclimated animals, resting metabolic rate was measured in awake animals at 30 °C. In addition, NE-stimulated (1 mg NE/kg body weight in saline, (-) arterenol bitartrate, intraperitoneally administered) energy expenditure was evaluated in anaesthetized (pentobarbital, 90 mg/kg) animals at 33 °C. Animals were allowed to recover from NE administration for 2–3 h at 30 °C. The mice were then rehoused at their acclimatisation temperature for 1 wk prior to tissue collection for gene and protein expression analysis to avoid effects of NE on gene expression. Oxygen consumption in conscious animals was followed for 3 h using an open circuit system with a chamber volume of 3 l and a flow rate of 1 l/min (Somedic, Hörby, Sweden). This system allowed the ambient temperature of the instruments to be adjusted between 5 °C and 40 °C, together with the volume and flow rates to optimise the system for the particular investigation. Oxygen consumption, carbon dioxide release, and ambient temperature data were collected every second minute via MacLab/2e (AD Instruments Pty. Ltd., Castle Hill, Australia). Resting metabolic rate was defined as the average of the lowest metabolic rates observed at three time points. Determinations in WT and PGC1 β KO mice were performed in alternating order.

Catherization and dobutamine treatment. Mice were anesthetized with isoflurane and underwent endotracheal intubation. The airway was connected to mouse ventilator (Model 687, Harvard Apparatus, Holliston, Massachusetts, United States) to control breathing. The oxygen flow rate was 1 l/min. The left jugular vein was identified and accessed by cut down method using a 25 G needle connected to a syringe with dobutamine hydrochloride (Sigma) that was mounted on a Standard Infuse/Withdraw Harvard 33 Twin Syringe Pump (Harvard Apparatus). A micromanometer-tipped catheter (Millar Instruments, Houston, Texas, United States) was then inserted into the left ventricle via right carotid artery, and hemodynamic measurements was obtained as described [28]. After obtaining baseline left ventricular pressure and heart rate readings, the dobutamine infusion was commenced. The initial infusion rate was 10 ng/min/g BW, with hemodynamic recordings taken at 2, 4, and 6 min. The infusion rate was then increased to 40 ng/min/g BW, and additional readings were obtained at 2, 4, and 6 min after the dose adjustment.

Tissue collection and RNA extractions. Mice were anaesthetised using isoflurane. Blood, tissues used for RNA, protein extraction, and histology were prepared as previously published [26,29].

Biochemical analysis. Enzymatic assay kits were used for determination of basic blood biochemical parameters as described in [26,29]. The size distribution profiles of serum lipoproteins were measured in pooled plasma samples using a high-performance liquid chromatog-

raphy system (HPLC), SMART, and a Superose 6 PC 3.2/30 column as described before [30].

Histological sample preparation and analysis. Tissue samples for morphological analysis were prepared according to published protocols [29]. For light microscopy, sections were stained with haematoxylin and eosin. For adipose tissue, images of each section were acquired using a digital camera and microscope (Olympus BX41, Olympus Corporation, Tokyo, Japan) and adipocyte area was measured using AnalySIS software (Soft Imaging System, Münster, Germany). Two fields from each section from gonadal, subcutaneous, and omental adipose tissue depots ($n = 7-8$ mice per genotype) were analysed to obtain the mean cell area per animal. For preparation of BAT, soleus muscle, and hearts for electron microscopy, mice were exsanguinated by perfusion with physiological saline containing 0.1% sodium nitrate until no blood was left. Mice were then perfused with 60–90 ml of fixative (3% glutaraldehyde and 1% formaldehyde in 0.1 mol/l 1,4-piperazine diethane sulfonic acid (PIPES) buffer (pH 7.4) containing 2 mol/l calcium chloride). Isotropic uniform random planes of section through the left ventricular wall in hearts were prepared using the orientator principle as described in [31]. Soleus samples were prepared at equal lengths along the long axis of the muscle. The blocks of tissue were sectioned in small fragments with a razor blade to <1 mm in one dimension and fixed by immersion at 4 °C for a further 3–4 h. Samples were then washed in 0.1 M PIPES and post-fixed in 1% osmium tetroxide, dehydrated in acetone, and embedded in Spurr's epoxy resin. Thin sections were obtained with a Leica UCT ultramicrotome (Leica Microsystems, Milton Keynes, United Kingdom) and examined with a transmission electron microscope (CM100, Philips, Netherlands).

Stereological assessment of mitochondria. Stereological assessments of mitochondrial volume fractions (V_v) and the surface density (S_v) of their inner and outer membranes in heart were performed as described in [31] and in [32].

Permeabilised tissue and isolated mitochondrial respiration studies. Isolation of mitochondria was performed in hearts and skeletal muscle from 10-wk-old male PGC-1 β mice and their WT littermates. Mice were killed by cervical dislocation. The hearts or hind limb skeletal muscle of four mice per genotype were pooled and immediately placed in ice-cold isolation medium (for hearts, 250 mM sucrose, 5 mM Tris, 2 mM EGTA at pH 7.4; for skeletal muscle, 100 mM KCl, 50 mM Tris, 2 mM EGTA at pH 7.4). Mitochondria were prepared essentially as described in [33]. Mitochondrial respiration was assessed in saponin-skinned soleus fibres prepared as in [14,34].

Measurement of proton conductance and ETC function in isolated mitochondria. The kinetics of proton conductance and ETC function were measured in mitochondria in the presence of oligomycin (1 μ g/ml), where that rate of respiration is directly proportional to the leak of protons across the mitochondrial inner membrane rather than a combination of ADP phosphorylation and proton leak. Mitochondrial function was assessed as described previously [35,36].

Quantitative RT-PCR analysis of gene expression. Total RNA was isolated from tissues as described and reverse-transcribed using the SuperscriptII kit (Invitrogen, Frederick, Maryland, United States) or Hi-Capacity cDNA archive kit (Applied Biosystems, Foster City, California, United States), following the manufacturers protocol. Oligonucleotide primers and TaqMan probe were designed using Primer Express, version 2.0 (Applied Biosystems). Primer and probe sequences, together with gene abbreviations, can be found in Tables S4–S6.

Microarray analysis. Male 14-wk-old mice were killed and dissected as above. The tissues were extracted for RNA as above and purified using the RNA clean-up protocol from the RNeasy Mini Kit (Qiagen Ltd, Crawley, UK). RNA was quantified spectroscopically at 260 nm using a GeneQuant Nucleotide calculator (Amersham Biosciences, Little Chalfont, UK) and checked for integrity on a 1% TBE gel using ethidium bromide staining. cDNA was amplified from total RNA using template-switching PCR and labeled with Cy3 or Cy5 dyes as previously described [37]. Binomial pathway enrichment analysis was then performed. A more detailed protocol can be found in Protocol S1. Raw data from the analysis are presented in Dataset S1 (pathway comparison) and Dataset S2 (raw data from the chip analysis).

Mitochondrial isolation, protein extraction, and Western analysis. Female 15-wk-old chow-fed mice were anaesthetised using isoflurane and killed by cervical dislocation and heart removal. BAT, heart, and soleus muscle tissue was removed and either snap-frozen in liquid nitrogen or used to prepare a mitochondrial extract as described in Protocol S1. In general, 10 μ g of total lysate or 3 μ g of mitochondrial preparation was separated by SDS-PAGE on 14%

gels. After transfer, the membranes were cut and placed in blocking buffer (5% powdered milk in 1 \times PBS and 0.1% Tween-20). We used anti-OxPhos complex I (α -subcomplex 9) and anti-OxPhos complex III (Fe-S core protein) (Molecular Probes, Carlsbad, California, United States) and anti-succinate dehydrogenase subunit B, anti-Cox4, and anti-ATP synthase β -subunit from Abcam, Cambridge, UK. All primary antibodies were used at ratios of 1:2,000, except anti-Cox4, which was used at 1:20,000. Goat anti-mouse horseradish peroxidase secondary antibody (Pierce, Rockford, Illinois, United States) was used at 1:40,000 for all blots, the membranes were reassembled, and the proteins detected using the ECL-Plus system (Amersham Biosystems). Films were scanned and analysed using NIH Image 1.34s.

Statistical analysis. The data presented here were analysed using the Student *t*-test or analysis of variance (ANOVA) with post-hoc tests on the program StatView Version 4.5 (Abacus Concepts, Berkeley, California, United States). Data are presented as mean \pm SEM unless stated. $p < 0.05$ was considered significant. The significance levels displayed on figures are as follows: * indicates $p < 0.05$, ** indicates $p < 0.01$, *** indicates $p < 0.001$.

Supporting Information

Dataset S1. Data Used for the Comparative Pathway Analysis of BAT, Heart, and Liver Tissues Using KEGG and KEGG2 Pathways

Found at DOI: 10.1371/journal.pbio.0040369.sd001 (62 KB XLS).

Dataset S2. Raw Data Text Files from the Spotted Array Experiments on Heart, Liver, and BAT Used in the Comparative Pathway Analysis

Found at DOI: 10.1371/journal.pbio.0040369.sd002 (3.2 MB XLS).

Figure S1. Size Distribution of Adipocytes from WT and PGC1 β KO Mice

Two fields from each section from (A) omental WAT, (B) subcutaneous WAT, and (C) female gonadal WAT depots (age 24 wk, $n = 7$ –8 mice per genotype) were analysed to obtain the mean cell area per animal.

Found at DOI: 10.1371/journal.pbio.0040369.sg001 (43 KB PPT).

Figure S2. Histological Sections of Tissues

Sections are as follows: BAT (A and B), liver (C and D), soleus muscle (E and F), pancreatic sections stained for glucagon (G and H), or pancreatic sections stained for insulin (I and J). A representative section from WT (A, C, E, G, and I) or PGC1 β KO (B, D, F, H, and J) are shown, $n = 6$.

Found at DOI: 10.1371/journal.pbio.0040369.sg002 (1.7 MB PDF).

Figure S3. Deletion of PGC-1 β Does Not Affect Insulin Sensitivity

Mice were placed on normal diet or HFD for 13 wk. GTTs (left panels) or ITTs (right panels) were performed on the mice at 16 wk of age. Plasma glucose levels of WT mice (open circles) and PGC1 β KO (solid circles) were measured during the protocol.

Found at DOI: 10.1371/journal.pbio.0040369.sg003 (115 KB PPT).

Figure S4. Expression of mRNAs Assessed on Soleus from 12-wk-Old Male WT (Black Bars) and PGC1 β KO (White Bars) Mice

Individual measurements were standardised using 18S, and the average of the WT group set to 1. $n = 6$ mice per group.

Found at DOI: 10.1371/journal.pbio.0040369.sg004 (34 KB PPT).

Figure S5. Assessment of Isolated Soleus Mitochondrial Function from WT and PGC1 β KO Mice

Soleus tissue was pooled from four WT mice (black bars) or four PGC1 β KO mice (white bars) and mitochondria isolated on five separate occasions ($n = 5$). Respiration states (A) were calculated using oxygen consumption rates in isolated mitochondria energised with succinate (4 mM). Respiratory control ratios (B) were determined for mitochondria as state 3 divided by state 4. Proton leak kinetics (C) were measured as described under Materials and Methods.

Found at DOI: 10.1371/journal.pbio.0040369.sg005 (35 KB PPT).

Figure S6. PGC-1 β Ablation Results in Few Changes in Gene Expression in Liver

Gene expression was analysed in 12-wk-old fed-state male WT (black bars) and PGC1 β KO (white bars) livers. Individual measurements are standardised using 18S and then the average of the WT group was set to 1. $n = 6$ mice per group.

Found at DOI: 10.1371/journal.pbio.0040369.sg006 (36 KB PPT).

Figure S7. Gene Expression of PGC-1 α and PGC-1 β (A) and for a Selection of Genes Involved with Fatty Acid and Cholesterol Handling in the Liver (B) in 8-wk-Old Female Mice Fed Surwit Diet for 24 h

WT chow, black bars; WT Surwit HFD, white bars; PGC1 β KO chow, dark gray bars; PGC1 β KO Surwit HFD, light gray bars. Individual measurements are standardised using 36B4 and then the average of the WT chow group was set to 1. $n = 4$ –7 per condition.

Found at DOI: 10.1371/journal.pbio.0040369.sg007 (35 KB PPT).

Protocol S1. Supplementary Protocols

Found at DOI: 10.1371/journal.pbio.0040369.sd003 (99 KB DOC).

Table S1. WT and PGC1 β KO Mouse Parameters for Energy Intake and Faecal Output over 48 h

The food intake and energetic content of faeces from 12-wk-old male mice was determined over a 48-h period. $n = 5$ –8 per group.

Found at DOI: 10.1371/journal.pbio.0040369.st001 (21 KB DOC).

Table S2. WT and PGC1 β KO Tissue Weights in 14-wk-Old Male Mice

The data are presented both comparing raw weights and as tissue weight/body weight. Statistical comparison between WT and PGC1 β KO mice was performed using *t*-tests. $n = 6$ –8 per group. *p* values are shown where *p* is less than or equal to 0.2.

Found at DOI: 10.1371/journal.pbio.0040369.st002 (25 KB DOC).

Table S3. Comparison of KEGG Pathways Significantly Down-regulated in all Three Arrayed Tissues (Liver, BAT, and Heart)

RNA was isolated from 14-wk-old normal diet-fed male PGC1 β KO and WT mice and then analysed using spotted arrays as described in the Materials and Methods. Data from these chips were then analysed using for pathway changes using the KEGG pathway database. Pathways with only one changed gene were discounted. Data are displayed as pathway name followed by *p* value for the binomial test. A pathway *p* value of < 0.05 was considered significant.

Found at DOI: 10.1371/journal.pbio.0040369.st003 (22 KB DOC).

Table S4. Sequences for Taqman Primers and Probes

Sybr as a probe indicates the use of a Sybr-Green system instead of Taqman.

Found at DOI: 10.1371/journal.pbio.0040369.st004 (31 KB DOC).

Table S5. Sequences for Taqman Primers and Probes

Sybr as a probe indicates the use of a Sybr-Green system instead of Taqman.

Found at DOI: 10.1371/journal.pbio.0040369.st005 (29 KB DOC).

Table S6. Sequences for Taqman Primers and Probes

Sybr as a probe indicates the use of a Sybr-Green system instead of Taqman.

Found at DOI: 10.1371/journal.pbio.0040369.st006 (29 KB DOC).

Acknowledgments

The authors would like to thank all lab staff who performed mouse breeding and biochemical analyses at AstraZeneca and the University of Cambridge for this project. We wish to thank Jane Löfvenmark for invaluable help during the early stages of the project. We would like to thank the animal care staff at the institutions involved for their work on this project. We also thank Ian McFarlane, Lyn Carter and Jeremy Skepper for providing technical help.

Author contributions. C. Lelliott, G. Medina-Gomez, M. Snaith, B. Cannon, and A. Vidal-Puig conceived and designed the experiments. C. Lelliott, G. Medina-Gomez, N. Petrovic, A. Kis, H. Feldmann, M. Bjursell, N. Parker, M. Campbell, P. Hu, D. Zhang, S. Litwin, V. Zaha, K. Fountain, S. Boudina, M. Jimenez-Linan, M. Blount, M. Lopez, A. Meirhaeghe, M. Bohlooly-Y, and M. Strömstedt performed the experiments. C. Lelliott, G. Medina-Gomez, N. Petrovic, A. Kis, H. Feldmann, N. Parker, K. Curtis, K. Fountain, S. Boudina, M. Jimenez-Linan, M. Blount, M. Orešič, E. Abel, B. Cannon, and A. Vidal-Puig analyzed the data. K. Curtis, M. Bohlooly-Y, M. Snaith, and M. Orešič contributed reagents/materials/analysis tools. C. Lelliott, G. Medina-Gomez, M. Snaith, E. Abel, B. Cannon, and A. Vidal-Puig wrote the paper.

Funding. The work presented in this paper was supported by

grants from the British Heart Foundation, Wellcome Trust Integrative Physiology, and Diabetes Wellness Research Foundation (to AVP lab); NIH grants RO1HL73167 and UO1HL70525 from the National Institutes of Health and the Ben and Iris Margolis Foundation (to EDA - Established Investigator of the American Heart Association).

Support was from the European Union (DLARFID), the Swedish Research Council, and the Swedish Cancer Society (to BC lab).

Competing interests. The authors having affiliations to AstraZeneca are paid employees of this company.

References

- Spiegelman BM, Heinrich R (2004) Biological control through regulated transcriptional coactivators. *Cell* 119: 157–167.
- Puigserver P, Wu Z, Park CW, Graves R, Wright M, et al. (1998) A cold-inducible coactivator of nuclear receptors linked to adaptive thermogenesis. *Cell* 92: 829–839.
- Yoon JC, Puigserver P, Chen G, Donovan J, Wu Z, et al. (2001) Control of hepatic gluconeogenesis through the transcriptional coactivator PGC-1. *Nature* 413: 131–138.
- Wu Z, Puigserver P, Andersson U, Zhang C, Adelmant G, et al. (1999) Mechanisms controlling mitochondrial biogenesis and respiration through the thermogenic coactivator PGC-1. *Cell* 98: 115–124.
- Andersson U, Scarpulla RC (2001) Pgc-1-related coactivator, a novel, serum-inducible coactivator of nuclear respiratory factor 1-dependent transcription in mammalian cells. *Mol Cell Biol* 21: 3738–3749.
- Lin J, Puigserver P, Donovan J, Tarr P, Spiegelman BM (2002) Peroxisome proliferator-activated receptor gamma coactivator 1beta (PGC-1beta), a novel PGC-1-related transcription coactivator associated with host cell factor. *J Biol Chem* 277: 1645–1648.
- Meirhaeghe A, Crowley V, Lenaghan C, Lelliott C, Green K, et al. (2003) Characterization of the human, mouse and rat PGC1 beta (peroxisome-proliferator-activated receptor-gamma co-activator 1 beta) gene in vitro and in vivo. *Biochem J* 373: 155–165.
- Kressler D, Schreiber SN, Knutti D, Kralli A (2002) The PGC-1-related protein PERC is a selective coactivator of estrogen receptor alpha. *J Biol Chem* 277: 13918–13925.
- Lin J, Tarr PT, Yang R, Rhee J, Puigserver P, et al. (2003) PGC-1beta in the regulation of hepatic glucose and energy metabolism. *J Biol Chem* 278: 30843–30848.
- Kamei Y, Ohizumi H, Fujitani Y, Nemoto T, Tanaka T, et al. (2003) PPARgamma coactivator 1beta/ERR ligand 1 is an ERR protein ligand, whose expression induces a high-energy expenditure and antagonizes obesity. *Proc Natl Acad Sci U S A* 100: 12378–12383.
- Lin J, Yang R, Tarr PT, Wu PH, Handschin C, et al. (2005) Hyperlipidemic effects of dietary saturated fats mediated through PGC-1beta coactivation of SREBP. *Cell* 120: 261–273.
- Lin J, Handschin C, Spiegelman BM (2005) Metabolic control through the PGC-1 family of transcription coactivators. *Cell Metab* 1: 361–370.
- Lin J, Wu PH, Tarr PT, Lindenberg KS, St-Pierre J, et al. (2004) Defects in adaptive energy metabolism with CNS-linked hyperactivity in PGC-1alpha null mice. *Cell* 119: 121–135.
- Leone TC, Lehman JJ, Finck BN, Schaeffer PJ, Wende AR, et al. (2005) PGC-1alpha deficiency causes multi-system energy metabolic derangements: muscle dysfunction, abnormal weight control and hepatic steatosis. *PLoS Biology* 3: e101. DOI: 10.1371/journal.pbio.0030101.
- St-Pierre J, Lin J, Krauss S, Tarr PT, Yang R, et al. (2003) Bioenergetic analysis of peroxisome proliferator-activated receptor gamma coactivators 1alpha and 1beta (PGC-1alpha and PGC-1beta) in muscle cells. *J Biol Chem* 278: 26597–26603.
- Koo SH, Satoh H, Herzig S, Lee CH, Hedrick S, et al. (2004) PGC-1 promotes insulin resistance in liver through PPAR-alpha-dependent induction of TRB-3. *Nature Med* 10: 530–534.
- Wolfum C, Stoffel M (2006) Coactivation of Foxa2 through Pgc-1[beta] promotes liver fatty acid oxidation and triglyceride/VLDL secretion. *Cell Metab* 3: 99–110.
- Russell LK, Mansfield CM, Lehman JJ, Kovacs A, Courtois M, et al. (2004) Cardiac-specific induction of the transcriptional coactivator peroxisome proliferator-activated receptor gamma coactivator-1alpha promotes mitochondrial biogenesis and reversible cardiomyopathy in a developmental stage-dependent manner. *Circ Res* 94: 525–533.
- Lehman JJ, Barger PM, Kovacs A, Saffitz JE, Medeiros DM, et al. (2000) Peroxisome proliferator-activated receptor gamma coactivator-1 promotes cardiac mitochondrial biogenesis. *J Clin Invest* 106: 847–856.
- Arany Z, He H, Lin J, Hoyer K, Handschin C, et al. (2005) Transcriptional coactivator PGC-1 alpha controls the energy state and contractile function of cardiac muscle. *Cell Metab* 1: 259–271.
- Tiraby C, Tavernier G, Lefort C, Larrouy D, Bouillaud F, et al. (2003) Acquisition of brown fat cell features by human white adipocytes. *J Biol Chem* 278: 33370–33376.
- Golozoubova V, Hohtola E, Matthias A, Jacobsson A, Cannon B, et al. (2001) Only UCP1 can mediate adaptive nonshivering thermogenesis in the cold. *FASEB J* 15: 2048–2050.
- Golozoubova V, Cannon B, Nedergaard J (2006) UCP1 is essential for adaptive adrenergic nonshivering thermogenesis. *Am J Physiol Endocrinol Metab*: E350–357.
- Golozoubova V, Gullberg H, Matthias A, Cannon B, Vennstrom B, et al. (2004) Depressed thermogenesis but competent brown adipose tissue recruitment in mice devoid of all hormone-binding thyroid hormone receptors. *Mol Endocrinol* 18: 384–401.
- Soriano P (1999) Generalized lacZ expression with the ROSA26 Cre reporter strain. *Nature Genet* 21: 70–71.
- Medina-Gomez G, Virtue S, Lelliott C, Boiani R, Campbell M, et al. (2005) The link between nutritional status and insulin sensitivity is dependent on the adipocyte-specific peroxisome proliferator-activated receptor-gamma2 isoform. *Diabetes* 54: 1706–1716.
- Bohlooly YM, Olsson B, Bruder CE, Linden D, Sjogren K, et al. (2005) Growth hormone overexpression in the central nervous system results in hyperphagia-induced obesity associated with insulin resistance and dyslipidemia. *Diabetes* 54: 51–62.
- McQueen AP, Zhang D, Hu P, Swenson L, Yang Y, et al. (2005) Contractile dysfunction in hypertrophied hearts with deficient insulin receptor signaling: Possible role of reduced capillary density. *J Mol Cell Cardiol* 39: 882–892.
- Lelliott CJ, Lopez M, Curtis RK, Parker N, Laudes M, et al. (2005) Transcript and metabolite analysis of the effects of tamoxifen in rat liver reveals inhibition of fatty acid synthesis in the presence of hepatic steatosis. *FASEB J* 19: 1108–1119.
- Linden D, William-Olsson L, Ahnmark A, Ekroos K, Hallberg C, et al. (2006) Liver-directed overexpression of mitochondrial glycerol-3-phosphate acyltransferase results in hepatic steatosis, increased triacylglycerol secretion and reduced fatty acid oxidation. *FASEB J* 20: 434–443.
- Howard CV, Reed MG (1998) Unbiased stereology: Three dimensional measurement in microscopy. Oxford: Bios Scientific Publishers. 256 p.
- Mattfeldt T, Mall G, Gharehbaghi H, Moller P (1990) Estimation of surface area and length with the orientator. *J Microscopy* 159: 301–317.
- Rolfe DF, Hulbert AJ, Brand MD (1994) Characteristics of mitochondrial proton leak and control of oxidative phosphorylation in the major oxygen-consuming tissues of the rat. *Biochim Biophys Acta* 1188: 405–416.
- Saks VA, Veksler VI, Kuznetsov AV, Kay L, Sikk P, et al. (1998) Permeabilized cell and skinned fiber techniques in studies of mitochondrial function in vivo. *Mol Cell Biochem* 184: 81–100.
- Cadenas S, Echtay KS, Harper JA, Jekabsons MB, Buckingham JA, et al. (2002) The basal proton conductance of skeletal muscle mitochondria from transgenic mice overexpressing or lacking uncoupling protein-3. *J Biol Chem* 277: 2773–2778.
- Echtay KS, Esteves TC, Pakay JL, Jekabsons MB, Lambert AJ, et al. (2003) A signalling role for 4-hydroxy-2-nonenal in regulation of mitochondrial uncoupling. *EMBO J* 22: 4103–4110.
- Petalidis L, Bhattacharyya S, Morris GA, Collins VP, Freeman TC, et al. (2003) Global amplification of mRNA by template-switching PCR: Linearity and application to microarray analysis. *Nucleic Acids Res* 31: e142.